Neutrino cross section and mean free path in neutron stars in the framework of the Dirac-Hartree-Fock approximation

R. Niembro,[1] P. Bernardos,[2] M. López-Quelle,[3] and S. Marcos[1]
[1]*Departamento de Física Moderna, Facultad de Ciencias, Universidad de Cantabria, E-39005 Santander, Spain*
[2]*Departamento de Matemática Aplicada y Ciencias de la Computación, E.T.S.I.I.T., Universidad de Cantabria, E-39005 Santander, Spain*
[3]*Departamento de Física Aplicada, Facultad de Ciencias, Universidad de Cantabria, E-39005 Santander, Spain*
(Received 24 May 2001; published 10 October 2001)

A study of the neutral current reactions of neutrinos with the dense matter existing in the late cooling stages of protoneutron stars is carried out. The zero-temperature approximation is assumed at this stage and nondegenerate neutrinos are considered. The matter consists of neutrons, protons, electrons, and muons. The fraction of each component is determined once the charge neutrality and beta equilibrated neutrino-free matter conditions are fulfilled. Several nuclear models are used, all inside a Dirac-Hartree or Dirac-Hartree-Fock approximations. These are a σ-ω model and three σ-ω-π-ρ models that differ in the coupling forms used for the πN and σN interactions. The neutrino mean free path is decreased in the Dirac-Hartree-Fock approximation from that obtained in the Dirac-Hartree approach by about 2–3 times at high densities. Some kind of consensus is found for the various models considered in the Dirac-Hartree-Fock approach in spite of their different foundations. Neutrino propagation is quite sensitive to the behavior of the relativistic nucleon effective mass. The dependence on the compression modulus and symmetry energy is also investigated.

DOI: 10.1103/PhysRevC.64.055802 PACS number(s): 13.15.+g, 21.60.Jz, 97.60.Jd, 26.60.+c

I. INTRODUCTION

Neutrino emission from newly formed neutron stars (NSs) in supernova explosions until later cooling phases plays an important role in describing their evolution and structure [1]. The most important component in the transport of neutrinos is the neutrino opacity [2]. It strongly depends on the interactions among the constituents of the NS, the composition of the star also affects the opacity. To study this fundamental process one key aspect involves the description of the interacting NS matter. Relativistic nuclear models provide an adequate framework to carry out this task, because of the supranuclear densities achieved in these systems.

Earlier work on neutrino opacities can be found elsewhere (Refs. [3–6], and references therein). Various scenarios and approximations are used throughout these papers concerning the models involved, as well as the components, temperatures, densities and type of neutrino reactions. In Ref. [7] noninteracting NS matter is considered. Sawyer [8] and Iwamoto and Pethick [9] show the relevance of the NS matter interactions upon neutrino propagation, in Ref. [9] calculations are performed in the framework of the Landau theory of Fermi liquids for pure neutron matter. Horowitz and Wehrberger [3,10,11] evaluate the neutrino cross section within the relativistic framework in the mean field approximation. Reddy *et al.* [4–6] provide several nonrelativistic and relativistic developments along with different conditions of the NS matter. However, as far as we know, there is only one work which considers the effect of exchange interaction [12] on the neutrino propagation in a relativistic framework, and no one where the σ-ω-π-ρ mesons are considered in the Dirac-Hartree-Fock (DHF) approach. Inasmuch the Fock contribution of each meson, and particularly that of the pion, is rather significant in determining the nuclear matter properties, it is presumably the influence of the Fock terms on the neutrino diffusion. Further investigations in this context are necessary.

Concerning the nucleon-nucleon interaction, the nonrelativistic nuclear models of Skyrme type [5] have proven to be not very adequate for various reasons. Some models become unstable to spin fluctuations or violate causality at high densities. They present an unexpected and anomalous behavior, that is, the neutrino mean free paths are increasing functions with the nuclear density. The relativistic Hartree models in these previous works [4–6] repair this problem. Regarding the composition of the star, it is well known that relativistic Hartree models do not reproduce the symmetry energy satisfactorily and, as a consequence, the g_ρ coupling constant must be taken as a fitting parameter in these references.

Correlations in the relativistic random-phase approximation (RPA) due to σ, ω, and ρ mesons in Ref. [6] result in an increase of the neutrino mean free path of 1–2.5 times the relativistic Hartree results at high density. The wide variation comes from the Migdal parameter chosen which parametrizes a very-short-range repulsive interaction by modifying the pion propagator.

The mean field approximation is the usual starting point for relativistic field theory calculations. One of the questions we are interested in this work is to elucidate if the Fock contribution itself is important for the neutrino opacity calculation, without considering in principle any RPA correlations.

The ground state of a NS is reached once the temperature has fallen below a few MeV. This state is gradually reached from the later stages of the cooling phase. The system is then quite dense and cool, so that the zero-temperature approximation is valid. The period of the previous stage, where neutrinos are trapped in a hot dense protoneutron star, is extremely short in comparison with the later stage. It is obvious that experimental data will be more easily collected in this period than in any other one [13]. We focus our development

on this scenario and consider the system made up by neutrons, protons, electrons, and muons. We are aware that a substantial amount of strange matter may be present in this cooling phase of the NS [5]. The neutrino scattering mean free path decreases because the large contribution of the Σ^- to the neutrino cross section through its large vector coupling $|C_V| \simeq 2$. In our neutrino-free scenario at zero temperature the direct URCA reaction $n + \nu_e \rightarrow e^- + p$ is kinematically possible for low-energy neutrinos at and above a threshold density when the proton fraction exceeds $\frac{1}{9}$ [14]. In the presence of muons, the proton fraction is slightly larger. Despite kinematical restrictions the absorption reaction dominates over the scattering reaction for densities up to about two times the saturation density for the nonrelativistic and relativistic models studied in Ref. [5]. To simplify the development we focus on the neutral current reactions as a first stage without considering strange matter effects. In fact one of the main motivations for our study is to compare the results from the different models, in the DHF approach, in order to detect whether some kind of pattern might appear which would allow a generic description of the neutrino propagation, as far as possible, model independent. To accomplish this goal it is enough to consider this simplified picture of the problem.

The only output required from the models to obtain the neutrino cross sections or the mean free paths are their nucleon self-energies and Fermi momenta. However, the discrepancies among the models are very large concerning the former quantities. On the other hand, no nuclear equation of state has yet been obtained to describe the nuclear matter from ordinary densities to extreme ones. Therefore some fundamental questions appear: Are these uncertainties large enough to make the results meaningless? Which are the observables of the NS matter to which neutrino propagation is more sensitive? Or equivalently, what can we learn about the behavior of dense matter that makes up NS from the neutrino signal? The aim of this work is to find some clues to answer these questions.

The paper is organized as follows. In Sec. II we outline the relativistic HF nuclear models which will be used throughout this work. Section III is devoted to describing the procedure to calculate the cross section and mean free path of the neutrino in the DHF approach. Some equations which complete this section are included in the Appendix. In Sec. IV we calculate the neutrino transport parameters, and elucidate the differences observed among the models, as well as their dependence on the nuclear density and initial neutrino energy. Finally, some conclusions are drawn about the sensitivity of the neutrino signal to the nuclear model observables.

II. DESCRIPTION OF THE NUCLEAR MODELS

For the sake of self-consistency we briefly describe the nuclear models applied in this study. More information about them can be found elsewhere [15–17].

The general Lagrangian that includes the four models reads

$$\begin{aligned}\mathcal{L} = {} & \overline{\psi}(i\gamma_\mu\partial^\mu - M - \hat{m}g_\sigma\sigma - g_\omega\gamma_\mu\omega^\mu)\psi - \overline{\psi}\Big(zig_\pi\gamma_5\vec{\pi}\cdot\vec{\tau} \\ & + (1-z)\frac{f_\pi}{m_\pi}\gamma_5\gamma^\nu\partial_\nu\vec{\pi}\cdot\vec{\tau}\Big)\psi - \overline{\psi}\Big(g_\rho\gamma^\mu\vec{\rho}_\mu\cdot\vec{\tau} \\ & + \frac{f_\rho}{2M}\sigma^{\mu\nu}\partial_\mu\vec{\rho}_\nu\cdot\vec{\tau}\Big)\psi + \frac{1}{2}(\partial_\mu\sigma\partial^\mu\sigma - m_\sigma^2\sigma^2) \\ & + \frac{1}{2}m_\omega^2\omega_\mu\omega^\mu - \frac{1}{4}F_{\mu\nu}F^{\mu\nu} + \frac{1}{2}m_\rho^2\vec{\rho}_\mu\cdot\vec{\rho}^\mu - \frac{1}{4}\vec{G}_{\mu\nu}\cdot\vec{G}^{\mu\nu} \\ & + \frac{1}{2}(\partial_\mu\vec{\pi}\cdot\partial^\mu\vec{\pi} - m_\pi^2\vec{\pi}^2) + \sum_{l=e^-,\mu^-}\overline{l}(i\gamma_\mu\partial^\mu - m_l)l,\end{aligned} \tag{1}$$

where

$$\vec{G}_{\mu\nu} = \partial_\nu\vec{\rho}_\mu - \partial_\mu\vec{\rho}_\nu \tag{2}$$

and

$$\hat{m} \equiv \left[1 - (1-h)g_\sigma\frac{\sigma}{M}\right]^{-1}. \tag{3}$$

ψ designates the nucleon field, and σ, ω, π, and ρ the four meson fields considered. The case $h=0$ corresponds to the pure derivative coupling whereas $h=1$ gives the linear scalar coupling. z is the mixing parameter between the pseudoscalar and pseudovector couplings for the pion. We use $z=0.25$ for the mixing model as one of the optimal values obtained from π-atoms and for elastic scattering of low-energy pions from nuclei [18].

The relativistic nuclear models are identified by the mesons and the sort of the meson-nucleon coupling that take part in them, a σ-ω model and three σ-ω-π-ρ models. The four models are applied in the DHF approximation. The first one, namely, the HF($\sigma+\omega$) model, is also applied in the Dirac-Hartree (DH) approach, the $H(\sigma+\omega)$ model, for comparison. Different coupling forms are used for the πN and σN interactions. One model includes the πN interaction with a pure pseudovector coupling form, namely, the HF(PV) model, whereas the two remaining models use a mixing of pseudoscalar and pseudovector couplings of the pion. A linear coupling in the scalar field is used except for the mixing models where both a linear scalar field and a derivative coupling in σ are considered. Hereafter, we shall refer to these last models as the HF(MIX) or the mixing model and HF(DER) or derivative model, respectively.

They all proceed from effective Lagrangians, where the σ and ω coupling constants are fitted to the nuclear matter saturation conditions $\rho_0 = 0.16$ fm^{-3} and $E/A(\rho_0) = -16.0$ MeV for the derivative model and $\rho_0 = 0.1484$ fm^{-3} and $E/A(\rho_0) = -15.75$ MeV for the three other models. Table I summarizes the values of the parameters and observables for all the models.

Monopole form factors with cutoff masses $\Lambda = 1140$ MeV are used for all mesons [19] in our linear models. However, in the derivative model, a genuine prescription

TABLE I. Adjusted σ and ω coupling constants of each model, defined by the used scalar coupling type h and mixing parameter z, and properties of symmetric nuclear matter at ρ_0. M^*/M is the nucleon scalar effective mass over the free value at the Fermi momentum, K is the NM compression modulus, and a_4 is the symmetry energy parameter. We choose $m_\sigma = 571$ MeV, $g_\rho^2/4\pi = 0.17$ for the derivative model and $g_\rho^2/4\pi = 0.55$ for the two other models. In both cases, the relation $f_\rho/g_\rho = 6.6$ is kept, as usual in OBEP potentials. ρ_c^{eq} is the critical density calculated in β equilibrium at which the ferromagnetic transition would take place and $\rho_B(0)$ is the maximum density in the center of the neutron star [16].

Model	h	z	$g_\sigma^2/4\pi$	$g_\omega^2/4\pi$	M^*/M	K (MeV)	a_4 (MeV)	ρ_c^{eq}	$\rho_B(0)$
H($\sigma+\omega$)	1		10.53	15.20	0.54	547	19.3		$4.0\rho_0$
HF($\sigma+\omega$)	1		9.64	12.52	0.51	589	31.1		$3.9\rho_0$
HF(PV)	1	0	9.22	9.79	0.56	434	34.0	$>\rho_B(0)$	$4.5\rho_0$
HF(MIX)	1	0.25	7.99	7.29	0.60	382	28.9	$4.1\rho_0$	$5.2\rho_0$
HF(DER)	0	0.25	4.27	3.76	0.72	268	33.6	?	$6.9\rho_0$

has been used to subtract the $\delta^3(r)$ contact interaction contribution to the potential energy [17] which is suppressed in realistic many body calculations by short-range correlations.

We consider a multicomponent system made up of neutrons, protons, electrons, and muons. Electrons and muons are included in the models as noninteracting particles since their interactions give small contributions compared to those of their free Fermi gas. The concentration of each component is determined once the charge neutrality and β equilibrated neutrino-free matter conditions at zero temperature are fulfilled. Figures 1–5 show the particle fractions obtained for each model as a function of the nuclear density. Differences in composition among the models arise from the differences in the symmetry energy values. The greater the symmetry energy the higher the proton concentration expected, as can be seen from Figs. 1–6.

For further interest Table I gives the critical density at which a ferromagnetic transition would take place inside a NS [16], as well as the maximum nuclear density value $\rho_B(0)$ allowed in the center of a NS. This value is calculated by solving the Tolmann-Oppenheimer-Volkoff equations [20], where hydrostatic equilibrium is guaranteed.

Figures 7 and 8 show the scalar and timelike self-energies for neutrons and protons, respectively, as functions of their respective momenta at $2\rho_0$ for all the models. The graphics illustrate the wide variation of these quantities among the models. In the DH approach, the self-energies are momentum independent, but not in DHF, where a strong dependence is shown for the neutron self-energies, particularly for the timelike ones. In the case of protons, a significant momentum dependence appears only for the mixing and derivative models. The vectorlike self-energy Σ_V is zero in the DH

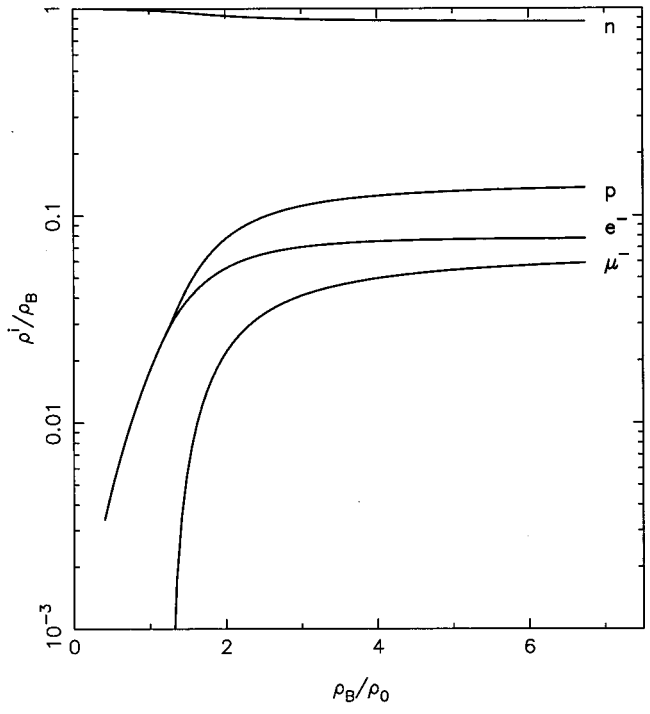

FIG. 1. Particle fractions obtained by imposing the β equilibrium at zero temperature as a function of the nuclear density in the Hartree ($\sigma+\omega$) model.

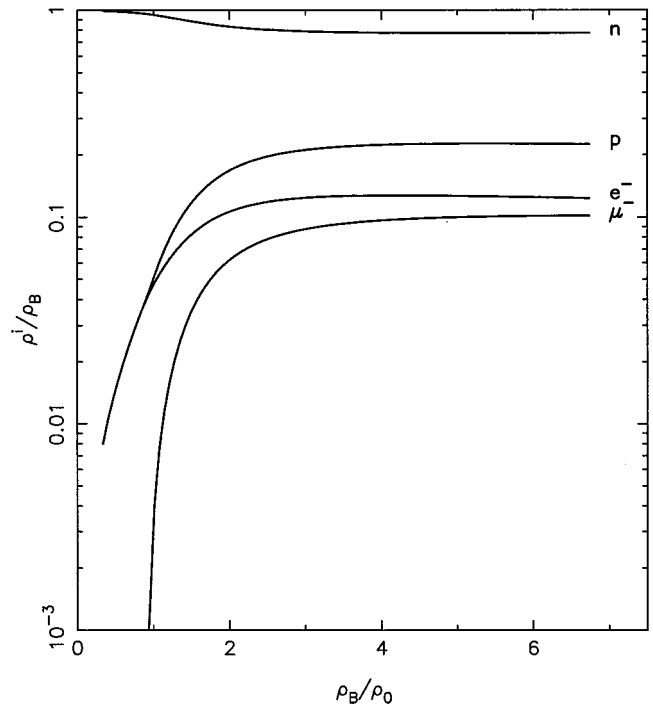

FIG. 2. Particle fractions obtained by imposing the β equilibrium at zero temperature as a function of the nuclear density in the HF($\sigma+\omega$) model.

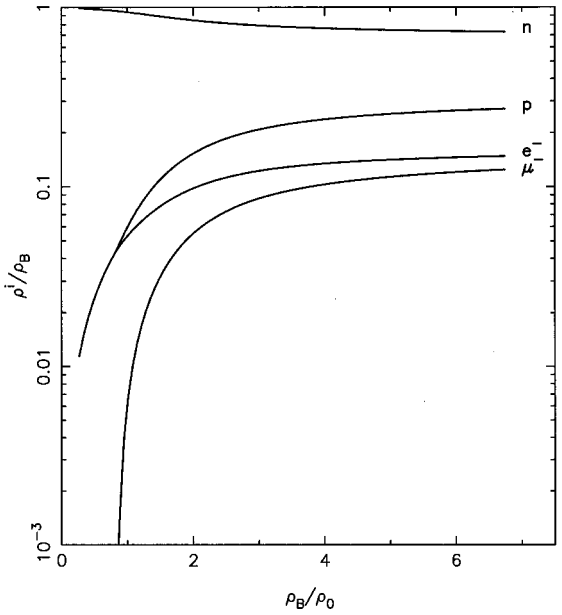

FIG. 3. Particle fractions obtained by imposing the β equilibrium at zero temperature as a function of the nuclear density in the HF(PV) model.

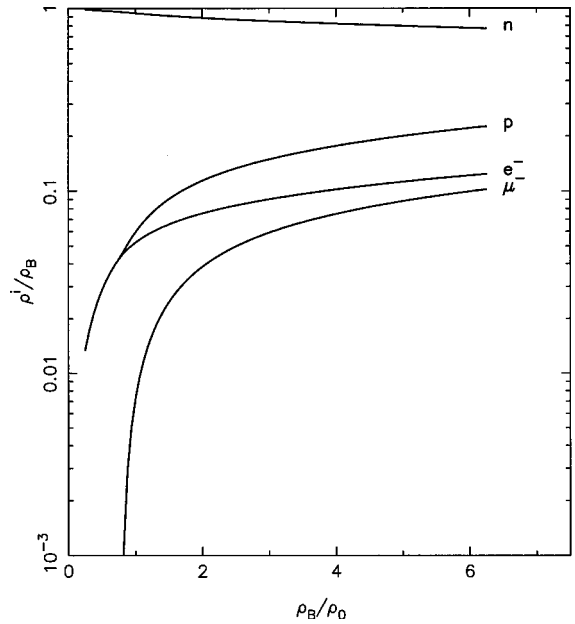

FIG. 5. Particle fractions obtained by imposing the β equilibrium at zero temperature as a function of the nuclear density in the HF(derivative) model.

approach and it is very small in the DHF approach with respect to the other self-energies, $|\Sigma_V| \simeq 5-30$ MeV at Fermi momentum.

III. NEUTRINO CROSS SECTION AND MEAN FREE PATH

We make use of an effective four-point coupling for the relevant interaction Lagrangian from Weinberg-Salam theory [21,22] in terms of a current-current interaction. It assumes the values of the momentum transferred much less than the masses of the weak gauge bosons and reads

$$\mathcal{L}^j_{\rm int} = \frac{G_F}{\sqrt{2}} [\bar{\nu}\gamma^\mu (1-\gamma_5)\nu](\bar{\psi} J^j_\mu \psi), \tag{4}$$

where ν is the neutrino spinor, while the other components

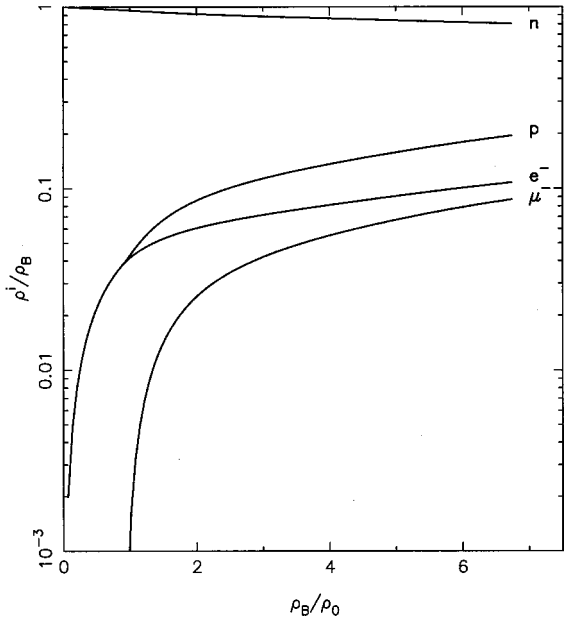

FIG. 4. Particle fractions obtained by imposing the β equilibrium at zero temperature as a function of the nuclear density in the HF(MIX) model.

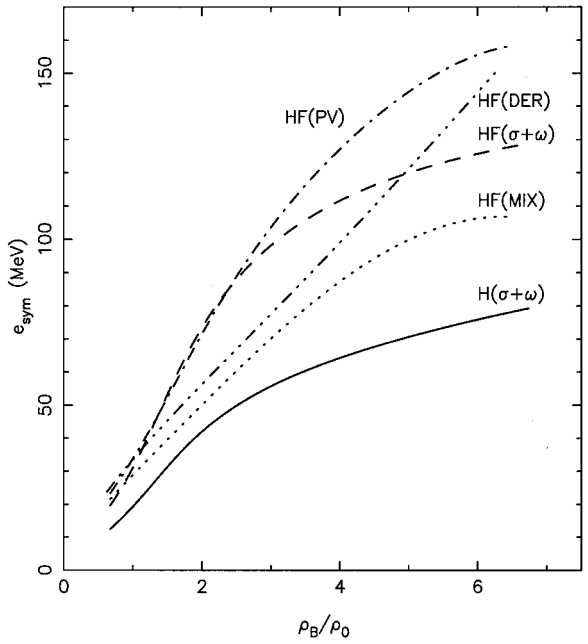

FIG. 6. Symmetry energy in MeV as a function of the nuclear density for the various models studied here.

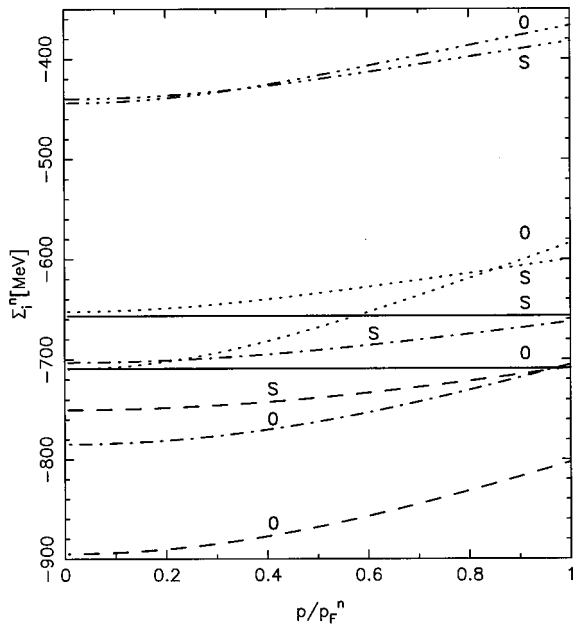

FIG. 7. Scalar and timelike neutron self-energies in MeV as a function of the neutron momentum at $2\rho_0$ for the models studied here. Full line refers to H($\sigma+\omega$) model, dashed line to HF($\sigma+\omega$) model, dashed-dotted line to HF(PV) model, dotted line to HF(MIX) model, and dashed-dot-dot-dot line corresponds to HF(DER) model.

are defined below. Index j serves to designate the different target particles: neutrons, protons, electrons, and muons in our case.

The neutrino differential cross section per volume may be expressed for elastic scattering in the following way [23]:

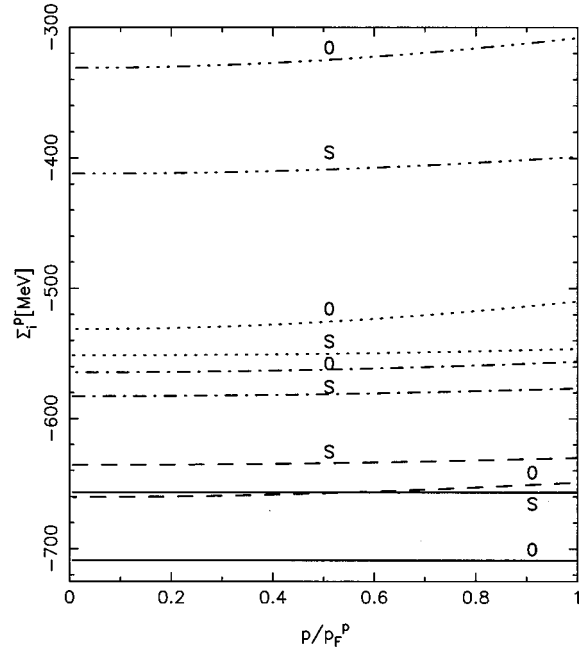

FIG. 8. Scalar and timelike proton self-energies in MeV as a function of the proton momentum at $2\rho_0$ for the models studied here. The meaning of the lines are the same as in Fig. 7.

$$\frac{1}{V}\frac{d^3\sigma}{d^2\Omega' dE'_\nu} = -\frac{G_F^2}{32\pi^2}\frac{E'_\nu}{E_\nu}\mathrm{Im}(L_{\mu\nu}\Pi^{\mu\nu}), \tag{5}$$

where E_ν and E'_ν are the initial and final neutrino energies, respectively,

$$L_{\mu\nu} = 8[2k_\mu k_\nu + (k\cdot q)g_{\mu\nu} - (k_\mu q_\nu + q_\mu k_\nu) \mp i\epsilon_{\mu\nu\alpha\beta}k^\alpha q^\beta] \tag{6}$$

is the neutrino tensor, with k the initial neutrino four-momentum and $q(q_0,\vec{q})$ the four-momentum transferred. $G_F = 1.023\times 10^{-5}/M^2$ is the weak coupling constant and $\Pi^{\mu\nu}$ is the polarization tensor. The latter embodies the description of the nuclear and lepton systems and is defined for each target particle specie as

$$\Pi^j_{\mu\nu}(q) = -i\int \frac{d^4}{(2\pi)^4}\mathrm{tr}\{G^j(p)J^j_\mu G^j(p+q)J^j_\nu\}, \tag{7}$$

$j = n,p,e^-,\mu^-$. $G(p)$ is the target particle propagator and $p(p_0,\vec{p})$ the corresponding initial four-momentum. In the case of the nucleon at the neutron or proton Fermi momenta $p_F^{n,p}$, the propagator in the DHF approximation reads as follows:

$$G^{n,p}(p) = (\not{p}^*_p + M^*_p)\left\{\frac{1}{p^{*2}_p - M^{*2}_p + i\epsilon} + \frac{i\pi}{E^*_p} \times \delta(p^*_0 - E^*_p)\,\theta(p_F^{n,p} - |\vec{p}|)\right\}, \tag{8}$$

where subindex p means momentum dependence. $E^*_p = \sqrt{\vec{p}^{*2}_p + M^{*2}_p} = E_p + \Sigma_0(p)$ is the nucleon effective energy with $M^*_p = M + \Sigma_S(p)$ being the nucleon scalar effective mass, $\vec{p}^*_p = \vec{p} + (\vec{p}/|\vec{p}|)\Sigma_V(p)$ the nucleon effective momentum and $\Sigma_S(p)$, $\Sigma_0(p)$, and $\Sigma_V(p)$ are the scalar, timelike, and spacelike self-energies, respectively. The electron and muon propagators have similar expressions to Eq. (8) for the nucleons when the starred quantities are replaced by the free ones.

Substituting the currents $J^j_\mu = \gamma^\mu(C^j_V - C^j_A\gamma_5)$ and J^j_ν into equation of polarization (7), one can decompose it into vector, axial, and vector-axial contributions. That is to say (particle specie index omitted for simplicity)

$$\Pi_{\mu\nu} = C_V^2\Pi^V_{\mu\nu} + C_A^2\Pi^A_{\mu\nu} - 2C_VC_A\Pi^{VA}_{\mu\nu}. \tag{9}$$

The neutral vector and axial coupling constants C_V and C_A for each particle species are given in Table II.

We emphasize that no analytical solution exists for the polarization tensor $\Pi_{\mu\nu}$ because of the momentum dependence of the self-energies in the DHF approach. After substitution of the Dirac particle propagators of Eq. (8) in Eq. (7) and then in Eq. (9) (Dirac sea effects were not considered) and contour integration over the p_0 complex plane, the following expression is obtained in a frame where $\vec{q}(0,0,q)$:

TABLE II. Neutral-current vector and axial couplings in terms of the Weinberg angle θ_w (with $\sin^2\theta_w=0.223$) and the nucleon axial coupling constant g_A (Gaillard and Sauvage). Neutral current couplings with nucleons of all neutrino species, including antineutrinos, are identical, i stands for e^--, μ^--, or τ^--type neutrinos.

Reaction	C_V	C_A
$\nu_i+n\rightarrow\nu_i+n$	$-1/2$	$-g_A/2$
$\nu_i+p\rightarrow\nu_i+p$	$1/2-2\sin^2\theta_w$	$g_A/2$
$\nu_e+e^-\rightarrow\nu_e+e^-$	$1/2+2\sin^2\theta_w$	$1/2$
$\nu_e+\mu^-\rightarrow\nu_e+\mu^-$	$-1/2+2\sin^2\theta_w$	$-1/2$

$$\mathrm{Im}\,\Pi_{\mu\nu}(q)=\frac{1}{2\pi}\int\frac{dpdxp^2}{E_p^*E_{p'}^*}F_{\mu\nu}\theta(p'-p_F)\,\theta(p_F-p)\times\delta[E_p^*-E_{p'}^*-\Sigma_0(p)+\Sigma_0(p')+q_0]. \tag{10}$$

In this equation $x=\cos\alpha$, α being the angle between the momentum transfer $\vec{q}$ and the initial target particle momentum $\vec{p}$. p' is the notation used for $|\vec{p}+\vec{q}|$ for brevity. $F_{\mu\nu}$ groups together traces of Dirac matrices, and is described for each type of contribution (vector, axial, and vector-axial) in the Appendix. θ functions in Eq. (10) show that the scattering proceeds from the Fermi sea to the unoccupied levels on top of it.

It is convenient, for computational reasons and to clarify the physical insight, to reduce the integral into a one-dimensional one. This can be achieved by using the δ function regarded as a function of x. We designate by $g(x)$ the argument of the δ in Eq. (10). It is also necessary to incorporate the constraint $|x|\leqslant 1$. A straightforward manipulation transforms Eq. (10) into

$$\mathrm{Im}\,\Pi_{\mu\nu}(q)=\frac{1}{2\pi}\int\frac{dpp^2}{E_p^*E_{p'}^*}F_{\mu\nu}\theta(p'-p_F)\times\theta(p_F-p)\left.\frac{\delta(x-x_j)}{|g'(x_j)|}\right|_{g(x_j)=0,|x_j|\leqslant 1}, \tag{11}$$

where $|g'(x_j)|$ reads

$$|g'(x)|=\frac{pq}{E_{p'}^*}\left|\left[1+\frac{\Sigma_V(p')}{p'}+\left(1+\frac{\Sigma_V(p')}{p'}\right)\Sigma_V'-\frac{M_{p'}^*}{p'}\Sigma_S'-\frac{E_{p'}^*}{p'}\Sigma_0'\right]\right|. \tag{12}$$

Σ_S', Σ_0', and Σ_V' mean derivation with respect to $p'\equiv|\vec{p}+\vec{q}|$. Care must be taken in handling the momentum as well as the x dependence in the self-energies because of their influence on the neutrino diffusion. The zeros of $g(x)$ for a given value of p are calculated self-consistently with the values of the self-energies. $|g'(x)|$ may be expressed in terms of the density of states of the DH or DHF particle spectrum by

$$|g'(x)|=\frac{pq}{p'}\frac{dE_{p'}}{dp'}. \tag{13}$$

The physical significance of this term comes from its relation to the relativistic generalization of the effective mass $\tilde{M}=p[(dE/dp)^{-2}-1]^{1/2}$ [15,24], which might be considered as a model observable, that coincides with the nucleon scalar effective mass M^* in DH. As will be seen later, this magnitude has profound effects on the neutrino diffusion. One can easily infer the behavior of $|g'(x)|$ with momentum and density for DH and DHF. Thus, it is a well established result [15,16,25,26] of relativistic nuclear models that the single particle spectrum is smoother in DHF than in DH. This fact should be considered a peculiarity of all relativistic models. The variations of this quantity from one model to another signal the differences observed in their cross sections and mean free paths, as shall be seen later.

Finally, the contraction between the neutrino tensor and the polarizations given in Eq. (11), leads to the differential cross section

$$\frac{1}{V}\frac{d^3\sigma}{d^2\Omega' dE_\nu'}=\frac{G_F^2}{4\pi^3}\frac{E_\nu'}{E_\nu}q_\mu^2\sum_j\,[(C_{Vj}^2+C_{Aj}^2)(A\,\mathrm{Im}\,\Pi^{Vj}+\mathrm{Im}\,\Pi^{Tj})-C_{Aj}^2\,\mathrm{Im}\,\Pi^{Aj}+2C_{Vj}C_{Aj}B\,\mathrm{Im}\,\Pi^{VAj}], \tag{14}$$

where

$$\mathrm{Im}\,\Pi^{Vj}=\mathrm{Im}\,\Pi^{Lj}+\mathrm{Im}\,\Pi^{Tj},\quad A=\frac{2E_\nu(E_\nu-q_0)+q_\mu^2/2}{|\vec{q}|^2},\qquad B=2E_\nu-q_0, \tag{15}$$

and j refers to neutrons, protons, electrons, and muons.

In Eq. (11), the integrand may be regarded as formed by two factors, namely, one made up by both θ functions together with the δ one, and the other made up by $F_{\mu\nu}$ Dirac trace factor. The first one by itself is proportional to the number of ways a particle can move from inside the Fermi sea to outside while keeping the kinematical constraints. The second one, that is, the trace factor may be related to the barionic or leptonic current fluctuation associated to the weak interaction. In our scenario and for the models considered here, the most influential factor upon neutrino propagation is the first one. Therefore, in momentum space, it could be regarded as proportional to the volume of an annular region located in the vicinity of the intersection of two Fermi spheres constructed by points that fulfill the former conditions imposed by the θ and δ functions.

As the momentum transfers involved in these processes, and in particular in our scenario, are very small in comparison with the Fermi momenta of the particles, especially with the neutron one, the available phase space is very small. This fact reinforces the effects of the density of states. Likewise,

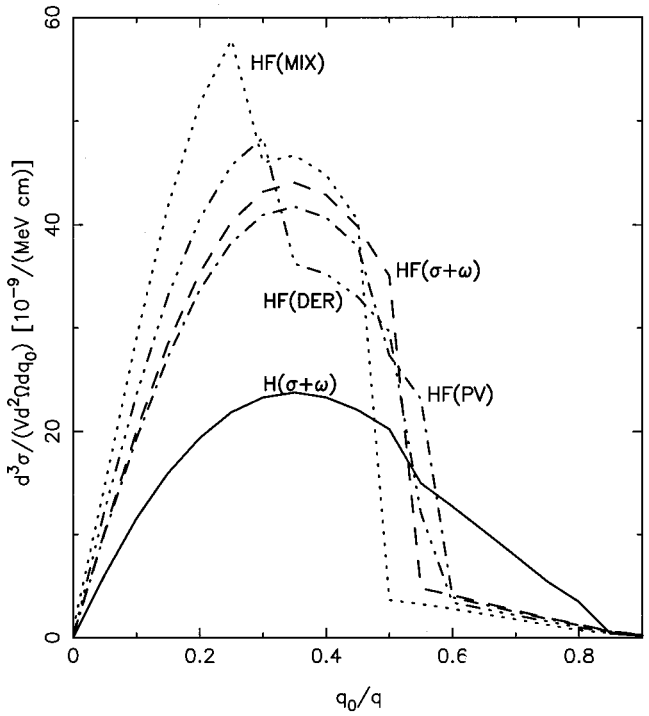

FIG. 9. Neutrino differential scattering cross section in charge-equilibrated matter at zero temperature in all the models. Contributions from neutrons, protons, electrons, and muons are summed up. $E_\nu = 5$ MeV and $q = 2.5$ MeV. The nuclear density chosen is $2\rho_0$.

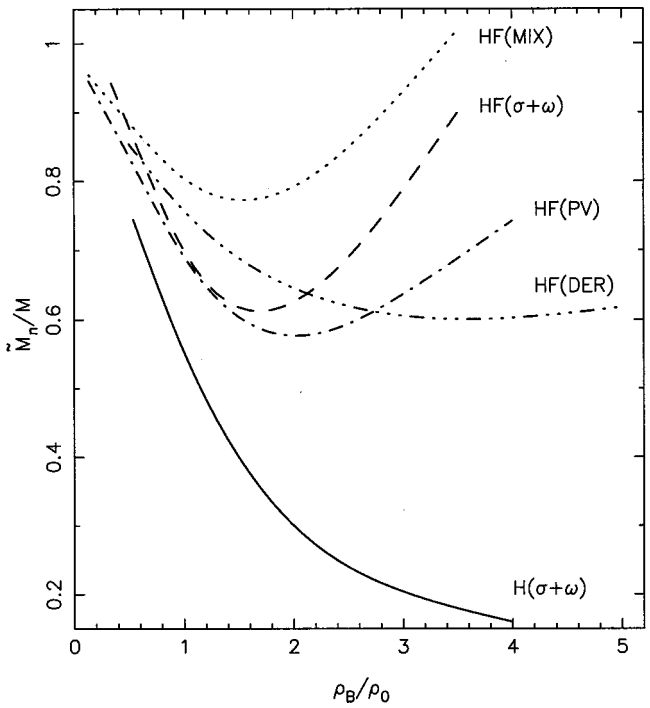

FIG. 10. Relativistic neutron effective mass calculated with the neutron fraction given by β equilibrium as a function of the nuclear density for the various models studied here.

the scattering processes are restricted to regions in the phase space very close to the Fermi surface. All these circumstances mean that a high degree of accuracy is required for the numerical integration.

The mean free path of neutrinos is easily calculated taking into account that neutrinos are nondegenerate at this stage, so that no blocking factor is necessary, and the zero-temperature approximation is valid. It is more suitable, for this calculation, to use as variables of integration the momentum and energy transfer, $|\vec{q}|$ and q_0, respectively. The mean free path λ as a function of the initial neutrino energy at a certain density is given by

$$\frac{1}{\lambda(E_\nu)} = \int_{q_0}^{2E_\nu - q_0} d|\vec{q}| \int_0^{2E_\nu} dq_0 \frac{|\vec{q}|}{E'_\nu E_\nu} 2\pi \frac{1}{V} \frac{d^3\sigma}{d^2\Omega' dE'_\nu}. \tag{16}$$

Equations (14) and (16) are used in the following section to produce our results.

IV. NUMERICAL RESULTS

As stated above, for our purpose and to simplify the development we concentrate on the scattering of ν_e. The absorption channel would be kinematically possible and presumably important in our DHF models up to about two times [three times for the HF(MIX) model] the nuclear matter saturation density. However, the small proton fractions of the H($\sigma+\omega$) model increase the threshold density for the absorption channel to be possible above four times ρ_0. Thus, in this case the scattering reactions are the prevailing ones that take place at this stage.

The extension to the scattering of $\overline{\nu_e}$ is straightforward, since the only modification with respect to ν_e is the opposite sign in the vector-axial term in Eq. (14), because of the neutrino helicity change. This contribution is very small in comparison with the vector and axial ones, so that the mean free path of $\overline{\nu_e}$ is approximately the same as that of ν_e. The ν- and $\overline{\nu}$- nucleon couplings are independent of the neutrino flavor while the ν- and $\overline{\nu}$- lepton ones are flavor dependent [5]. Therefore, the neutrino mean free path due to nucleons is the same for all flavor neutrinos. However, the neutral current vector coupling for ν_μ- and ν_τ-e^- scattering is much smaller than the corresponding to ν_e-e^-.

Typical initial neutrino energies for the cooling phase of a NS in the late stages are about $E_\nu = 5$ and 10 MeV. We calculate the neutrino differential cross section and mean free path at these E_ν with $|\vec{q}| = 2.5$ and 5 MeV, alternatively. In the following, the main results of this work are discussed. We stress the differences observed between DH and DHF approaches, as well as those arising from each model in turn.

(1) *Kinematical limits*. First, we focus on the neutrino cross sections. The maximum limits of q_0 at $|\vec{q}|$ constant with nonzero cross sections are accurately approximated by taking into account that $|\vec{q}|$ is small in relation with the target particle Fermi momentum and that the scattering involves the phase space very close to the surface of the Fermi sphere. From the energy conservation $E_{p'} = E_p + q_0$ and a Taylor expansion of $E_{p'}$ and E_p around p_F, the maximum value of q_0 for scattering with nucleons is found to be a function of the nucleon effective mass and Fermi momentum at fixed $|\vec{q}|$

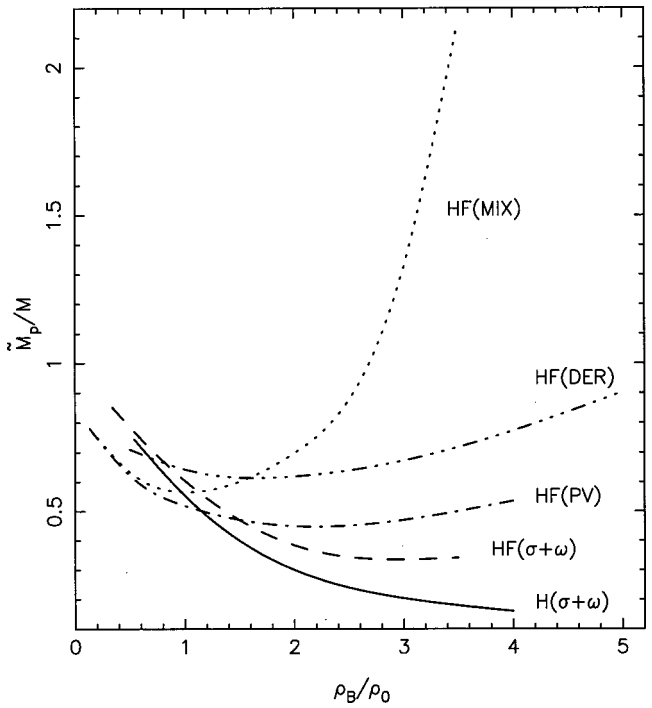

FIG. 11. Relativistic proton effective mass calculated with the proton fraction given by β equilibrium as a function of the nuclear density for the various models studied here.

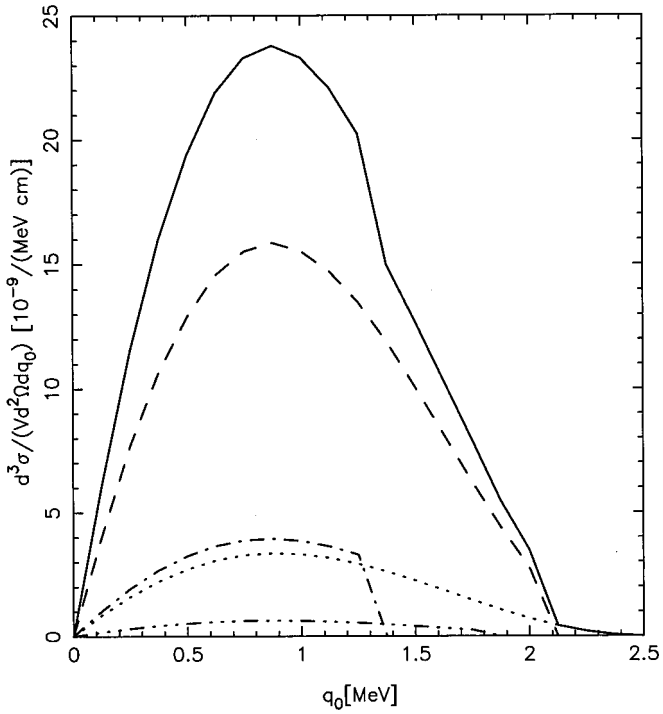

FIG. 12. Neutrino differential scattering cross section in charge-equilibrated matter at zero temperature in the Hartree $(\sigma+\omega)$ model. Contributions from neutrons (dashed line), protons (dashed-dotted line), electrons (dotted line), and muons (dashed-dot-dot-dot line) are displayed as well as the total contribution, at the nuclear matter density $2\rho_0$. $E_\nu = 5$ MeV and $q = 2.5$ MeV.

$$q_0^{\max} \simeq \frac{1}{\sqrt{(\tilde{M}/p_F)^2+1}}|\vec{q}|. \tag{17}$$

The p_F of electrons and muons is very much larger than their free masses, so that $q_0^{\max} \simeq |\vec{q}|$. The minimum value for q_0 is zero.

(2) *DHF versus DH*. Figure 9 shows the differential neutrino cross section obtained for scattering with neutrons, protons, electrons and muons at $2\rho_0$ for all the models. All the DHF results present a narrower width of the cross section versus the corresponding DH one. Moreover, an increase of the height of the cross section occurs in DHF models versus the DH model, while keeping a similar shape. The same qualitative results are obtained for higher nuclear matter densities, with bigger relative differences between the DHF models and the DH one.

This behavior is understood by means of the values of the neutron and proton effective masses, which are displayed in Figs. 10 and 11, respectively, for all the models considered here. The neutron effective mass in any DHF model is larger than the corresponding value in the DH model, and the values of $q_0^{\max}$ for both approximations are well reproduced by using Eq. (17). With regard to the value of the neutrino cross section, it is directly dependent on the nucleon effective mass [see Eqs. (11) and (12)]. The dominant contribution to the neutrino scattering cross section from neutrons, protons and muons arises from the axial contribution to Eq. (14), as one can see from the values of their axial coupling constants in Table II. The vector part is the most important contribution to the neutrino cross section coming from scattering with electrons.

Figures 12–16 show the contributions of each target particle to the differential neutrino cross section shown in Fig. 9, for each model at the nuclear matter density $2\rho_0$. Figures 17–21 are the corresponding ones at $3\rho_0$. The changes in the different models can be explained as a consequence of the behavior of the nucleon effective mass and the particle fractions given by the β equilibrium. Let us focus, first, on the DH and HF$(\sigma+\omega)$ results (Figs. 12 and 13). As Figs. 10 and 11 show, at $2\rho_0$ the DH effective masses lie below the DHF ones for neutrons and protons and they are closer to the last ones. Therefore, the growth for the neutrino cross section undergone in the DHF approach versus the DH one is larger for the neutron case than for the proton one. The composition of the NS is displayed for both approaches as a function of the density in Figs. 1 and 2. The neutron concentration is slightly decreased in DHF in comparison with DH and evidently the opposite is true for protons. One can easily verify with Eq. (17) which are the q_0 maxima in both models and for each component. The shift in $q_0^{\max}$ for neutrons to smaller values in HF$(\sigma+\omega)$ is more than compensated with the growth undergone in height of the cross sections for neutrons and protons. The net balance provides an enhancement of the DHF neutrino cross section versus the DH one. Electrons and muons play a minor role. This result has a direct effect on the neutrino mean free path as can be seen in Fig. 22. As the density increases, the gap between the DH and HF$(\sigma+\omega)$ effective masses increases, and it is more pronounced for neutrons than for protons, both cross sections following

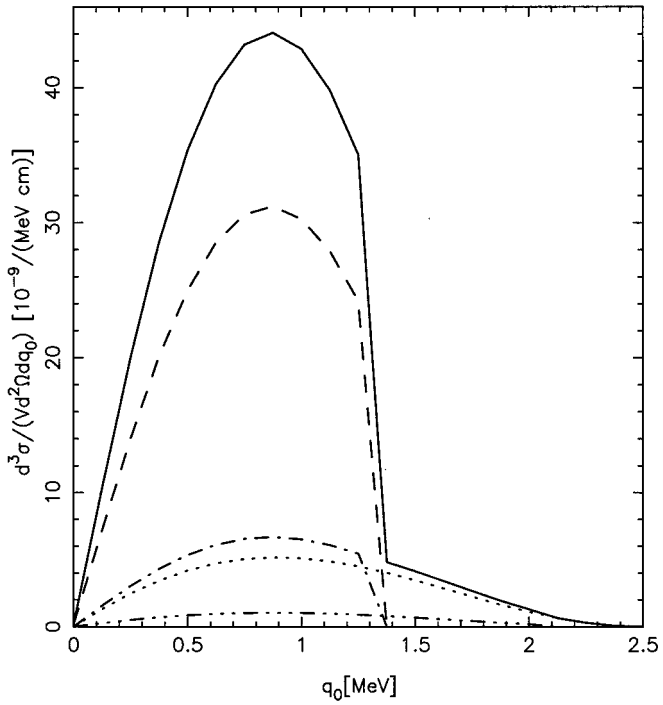

FIG. 13. Neutrino differential scattering cross section in charge-equilibrated matter at zero temperature in the HF($\sigma+\omega$) model. Contributions from neutrons (dashed line), protons (dashed-dotted line), electrons (dotted line), and muons (dashed-dot-dot-dot line) are displayed as well as the total contribution, at the nuclear matter density $2\rho_0$. $E_\nu=5$ MeV and $q=2.5$ MeV.

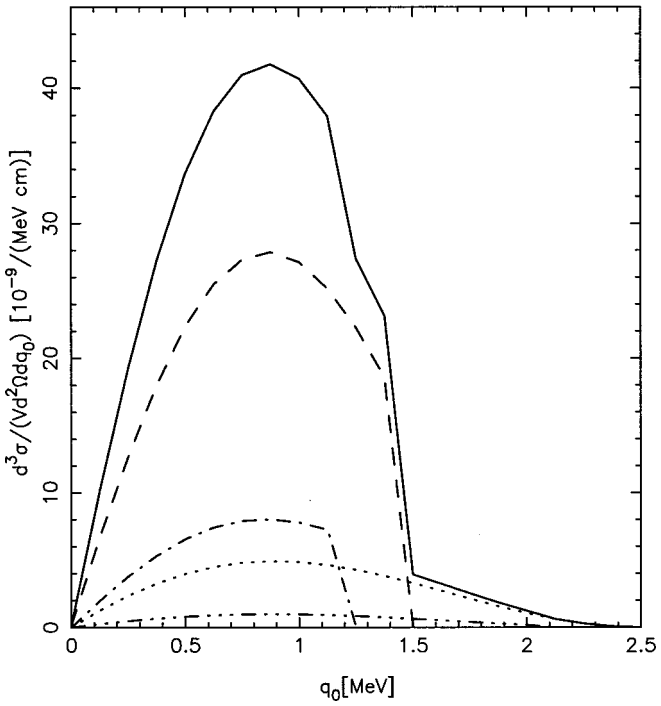

FIG. 14. Neutrino differential scattering cross section in charge-equilibrated matter at zero temperature in the HF(PV) model. Contributions from neutrons (dashed line), protons (dashed-dotted line), electrons (dotted line), and muons (dashed-dot-dot-dot line) are displayed as well as the total contribution, at the nuclear matter density $2\rho_0$. $E_\nu=5$ MeV and $q=2.5$ MeV.

the same pattern as their corresponding effective masses. Thus, the same qualitative behavior is observed at larger densities (see Figs. 17, 18, and 19), so that the same conclusions are still valid in this region.

(3) *Role of the isovector mesons*. The main effect of the isovector mesons π and ρ on the nuclear observables is to reduce in part the compression modulus, which is overestimated in the HF($\sigma+\omega$) model, as is shown in Table I. The tensor part of the ρ meson plays a dominant role in this effect. To analyze the consequences on the neutrino cross sections and mean free paths, we proceed as before, by inspecting in Figs. 10 and 11 the curves corresponding to the nucleon effective masses of both models, the HF($\sigma+\omega$) and HF(PV). At $2\rho_0$, the neutron (proton) effective mass of the pseudovector model lies below (above) that of the HF($\sigma+\omega$) model. The compositions of the NS for both models, Figs. 2 and 3, are very similar. Thus, the $q_0^{\max}$ for the cross sections are in fair agreement with Eq. (17), that is to say, it is increased for neutrons (decreased for protons), when going from the HF($\sigma+\omega$) model to the HF(PV) one, see Figs. 13 and 14. The height of the neutron and proton cross sections undergoes an opposite tendency to the corresponding widths. Therefore, a small diminution of the cross section is observed in the pseudovector model. The neutrino mean free paths for both models are displayed in Fig. 22 as a function of the nuclear density. No significant changes go through from one function to the other. The previous comparison provides some hints on the correlation between the mean free path and the compression modulus. Indeed, the saturation conditions are the same for both models since they are imposed in the fitting procedure. The symmetry energy parameter a_4 and nucleon scalar effective mass differ by about 10%, while the compression modulus undergoes a variation of 30%. The mean free path is rather insensitive to this change.

(4) *Effects of pseudoscalar coupling*. The mixing model is adequate to study the effect of the pseudoscalar coupling, which increases the magnitude and slopes of the self-energies when represented versus the nucleon momentum p, compared to the previous DHF models studied, see Figs. 7 and 8. The reduction of the compression modulus and the symmetry energy parameter are the main effects on the nuclear observables regarding the HF($\sigma+\omega$) and PV models, as can be seen in Table I. It is interesting to compare its outcome with respect to the HF(PV) model. At two times the saturation density, the neutron and proton effective masses are located above the corresponding pseudovector ones. By the same arguments stated previously, the cross section characteristics are easily understood. However, the most significant feature in this model is the tremendous increase in the proton effective mass, as shown in Fig. 11. Two consequences stem from this growth; on the one hand the enlargement of the ν-proton cross section, and on the other hand the reduction of the proton $q_0^{\max}$ value as the density

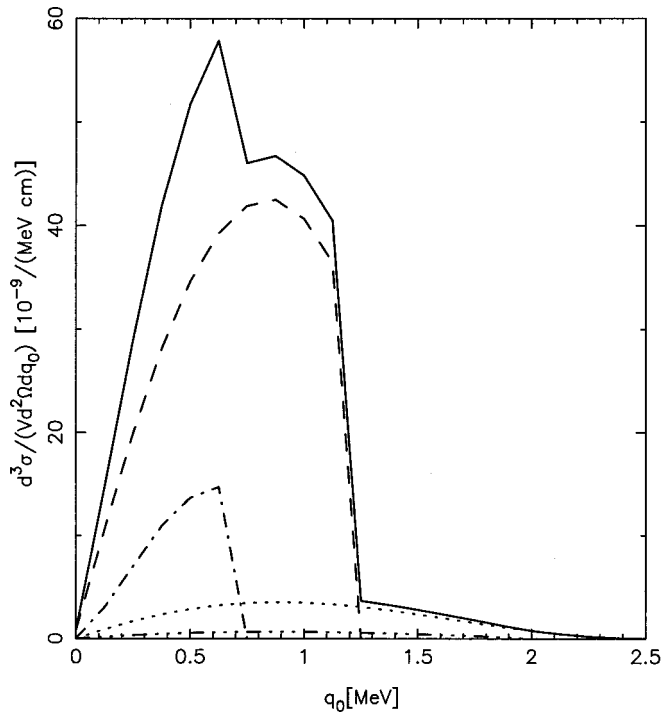

FIG. 15. Neutrino differential scattering cross section in charge-equilibrated matter at zero temperature in the HF (MIX) model. Contributions from neutrons (dashed line), protons (dashed-dotted line), electrons (dotted line), and muons (dashed-dot-dot-dot line) are displayed as well as the total contribution at the nuclear matter density $2\rho_0$. $E_\nu = 5$ MeV and $q = 2.5$ MeV.

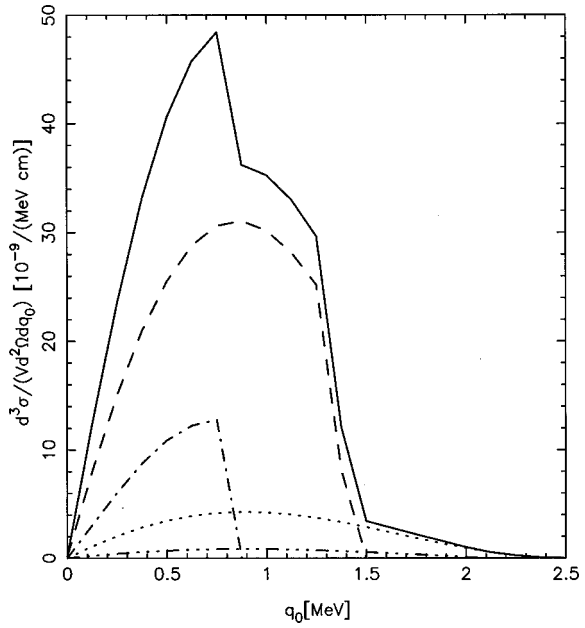

FIG. 16. Neutrino differential scattering cross section in charge-equilibrated matter at zero temperature in the derivative model. Contributions from neutrons (dashed line), protons (dashed-dotted line), electrons (dotted line), and muons (dashed-dot-dot-dot line) are displayed as well as the total contribution at the nuclear matter density $2\rho_0$. $E_\nu = 5$ MeV and $q = 2.5$ MeV.

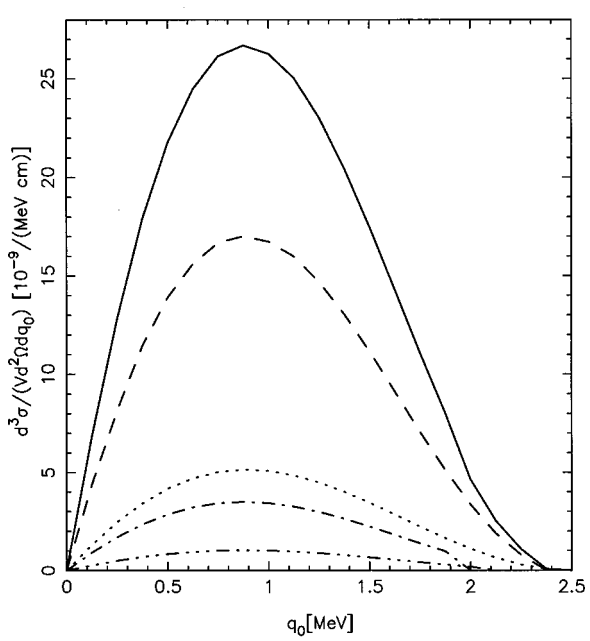

FIG. 17. The same as Fig. 12 for a nuclear density $\rho_B = 3\rho_0$ with the corresponding concentrations in charge-equilibrated matter.

increases. One can see the variation of these parameters with the nuclear density in Figs. 15 and 20. The symmetry energy influences the neutrino mean free path through its effect on the composition of the star. The mixing model and the H($\sigma + \omega$) model present small values of the symmetry energy, that is, small proton concentrations. As shown in Ref. [24], the exchange terms increase the values of the effective masses both for protons and neutrons with the density. This growth depends on the isospin asymmetry and the baryon specimen. The higher the asymmetry parameter, the greater

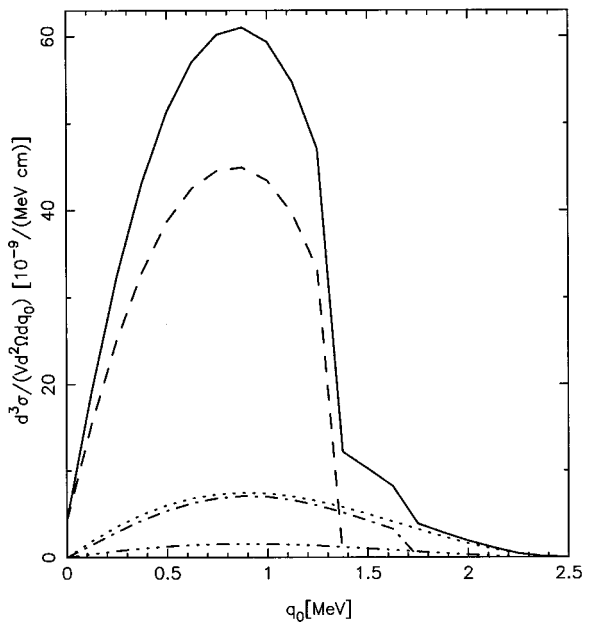

FIG. 18. The same as Fig. 13 for a nuclear density $\rho_B = 3\rho_0$ with the corresponding concentrations in charge-equilibrated matter.

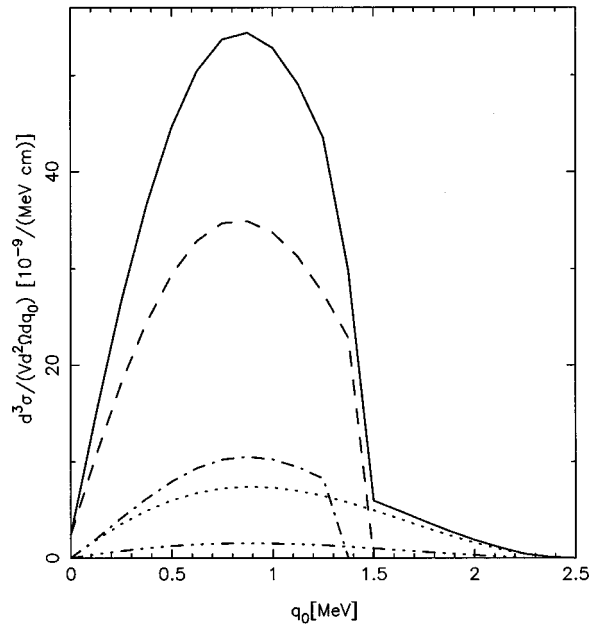

FIG. 19. The same as Fig. 14 for a nuclear density $\rho_B = 3\rho_0$ with the corresponding concentrations in charge-equilibrated matter.

the increase in the relativistic effective masses, being more pronounced for protons than for neutrons. We have checked for a pure pseudoscalar model ($z=1$) the tendency of this effect. In this case $a_4 = 27$ MeV, slightly lower than in our mixing model. The sharp increase of the proton effective mass with the density is moved towards lower values of ρ, about twice the ordinary nuclear density. The DH model has

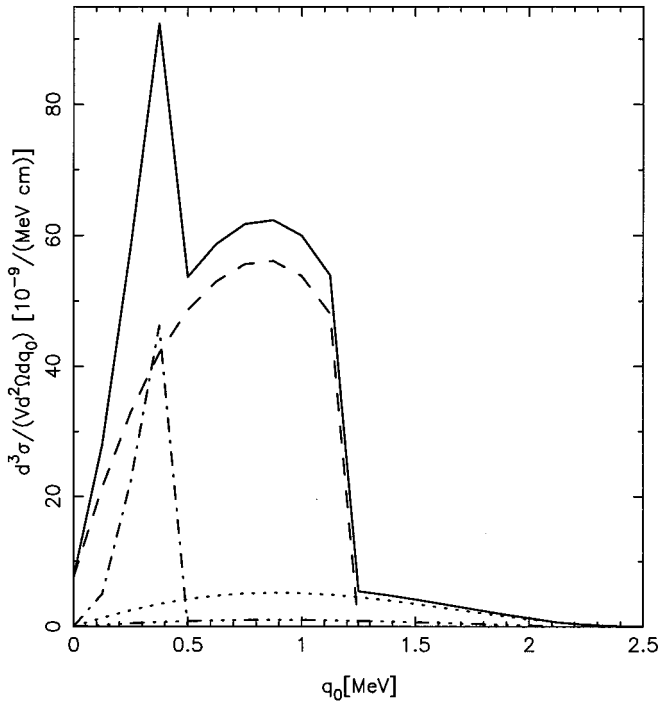

FIG. 20. The same as Fig. 15 for a nuclear density $\rho_B = 3\rho_0$ with the corresponding concentrations in charge-equilibrated matter.

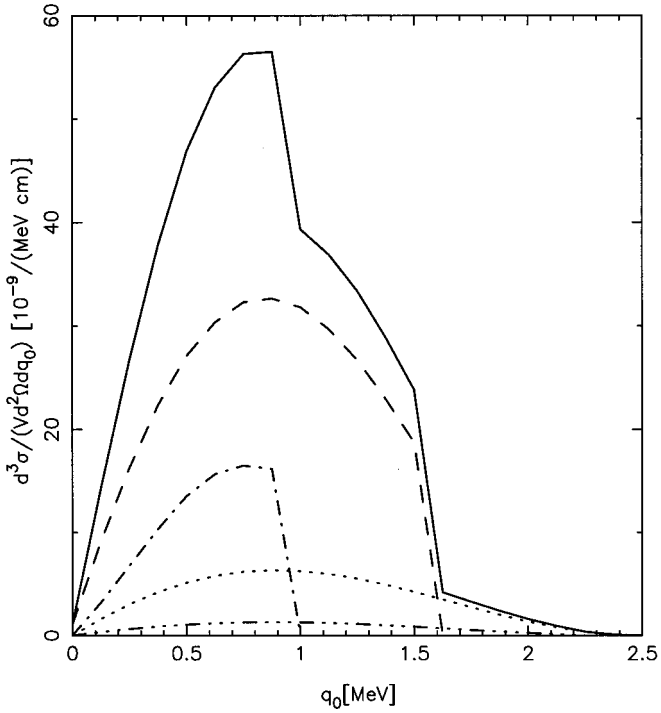

FIG. 21. The same as Fig. 16 for a nuclear density $\rho_B = 3\rho_0$ with the corresponding concentrations in charge-equilibrated matter.

the lowest a_4 parameter and, consequently, the smallest proton fraction. However, the effect of the rising of the effective masses with the baryon density, previously mentioned, is not observed. The reason is that the relativistic effective mass is equal to the scalar effective one, and the latter does not increase with the density, in contrast with the former as it is shown in Ref. [24]. The neutrino mean free path in the mixing model is shorter than in any other model, as displayed in Fig. 22. The protons are mainly responsible for this reduction.

(5) *Effects of the nonlinearities in the σ field*. Table I shows the drastic decrease in the nuclear matter compressibility, to a value within the range of accepted experimental values, and the increase in the scalar effective mass brought about by the derivative model with respect to the other descriptions. These features provide a good nuclear matter description, while conserving suitable behavior in finite nuclei concerning the spin-orbit splitting, due to the increase in the scalar effective mass [17]. The symmetry energy parameter is also well reproduced because of the ρ meson effect. At ρ_0 the neutrino differential cross section in the derivative model looks very similar to that of the mixing model. However, differences become significant as the density increases (Figs. 15 and 16) following the same trends as the corresponding effective masses. Height and width relations in the cross sections are again well reproduced by the same expressions used before. Beyond $2\rho_0$, the contrast between both models is more evident, as displayed in Figs. 20 and 21, not only due to the proton effective mass increase in the mixing model, which is absent in the derivative one, but also for the greater neutron effective mass. The heights of the ν-neutron and ν-proton cross sections approach each other, in the derivative

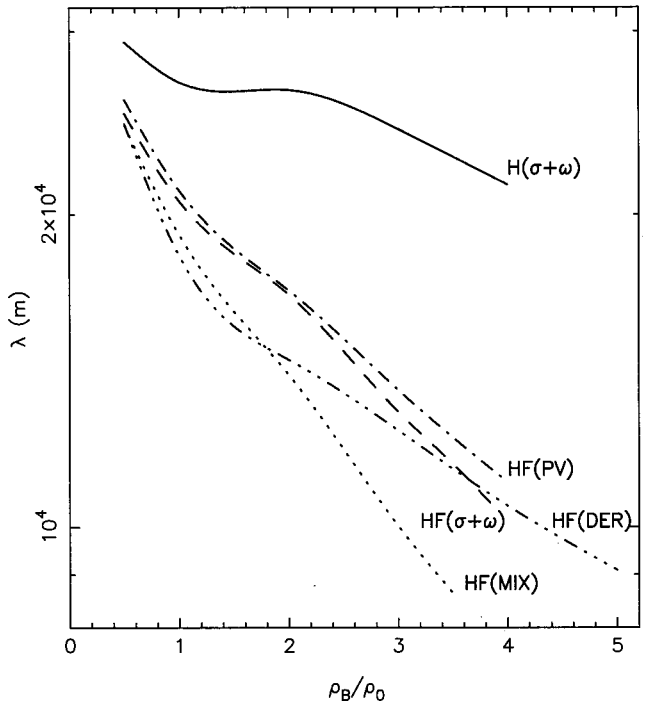

FIG. 22. Neutrino scattering mean free path as a function of the nuclear density for $E_\nu = 5$ MeV.

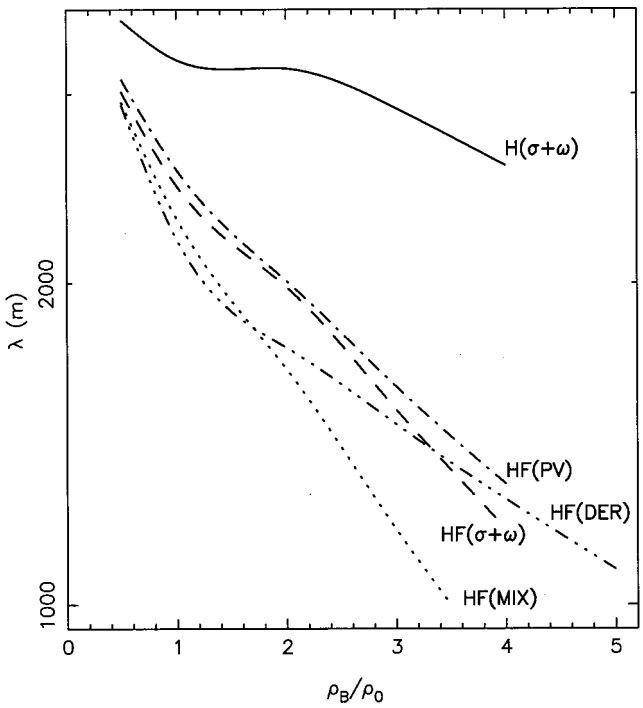

FIG. 23. Neutrino scattering mean free path as a function of the nuclear density for $E_\nu = 10$ MeV.

model, as the density increases. This fact is immediately deduced from the behavior of their respective effective masses as a function of the density. The neutrino mean free path obtained with the derivative model shows, as can be seen in Fig. 22, the smoothest function of the nuclear density in the high density interval. This is the most reliable model to trust in at high densities. For instance, the derivative model presents a better high density behavior than other nonlinear relativistic models that contain terms in σ^3 and σ^4 in the Lagrangian. In these models, the truncation of the nonlinear contributions yields an energy per particle that behaves as a polynomial of the density which sooner or later produces undesirable effects. In Fig. 23 the results of the neutrino mean free path with $E_\nu = 10$ MeV are shown. The same qualitative behavior is conserved as it is easily deduced from the expression of the cross section.

It is worth mentioning that the contribution of the vectorlike self-energies to the neutrino mean free path is not negligible. Although their absolute values are small in comparison with the other self-energies, their momenta dependence is significant and enters in Eq. (12) for the calculation of the neutrino cross section. The $q_0^{\max}$ of Eq. (17) is also changed a little. Thus, the neutrino mean free path at $2\rho_0$ decreases about 10% for the HF(DER) model when the vectorlike self-energies are removed. Different growths and signs of $\Sigma_V^{n,p}$ near the Fermi surface for the various DHF models influence in one sense or the opposite the neutrino mean free path, but in all the cases the variation is about 10% or less.

Up to the nuclear densities where the calculations of the neutrino mean free path are made, and within these models, the NS is stable and supposed to be spin symmetric (Table I). No ferromagnetic transition is expected for both H($\sigma+\omega$) and HF($\sigma+\omega$) models. The pseudovector model leads to a ferromagnetic transition that would describe an unstable star. That is to say, the critical density calculated in β equilibrium for the ferromagnetic transition to take place, would be larger than the maximum density, $\rho_B(0)$, in the center of the NS model.

However, the mixing model leads to a ferromagnetic transition at a critical density about four times ρ_0, which can occur inside a NS. Above this value of the density, the mean free path should be calculated for magnetized NS matter. Work is in progress in this direction. Regarding the derivative model, its soft equation of state leads to the greatest maximum density value $\rho_B(0)$ in the center of a NS of all the models.

V. CONCLUSIONS

In the present work we have for the first time used different relativistic DHF models to study neutrino propagation in NS. The astrophysical situation chosen is that of the late stages of the cooling of a protoneutron star. At this stage, the zero temperature approximation is plausible and the typical initial neutrino energies are around 5–10 MeV.

The Fock inclusion in the nuclear models has been found to be very important in the calculation of the neutrino mean free path. More complicated momentum and density dependences in the nucleon energy spectra are some of the new important features that appear in DHF models. Thus, the DH and DHF approaches yield very different neutrino mean free paths.

It is interesting to note that opposite corrections to the relativistic DH neutrino mean free path are obtained when

including RPA correlations or Fock interactions in the nuclear medium. At high densities, the former increases the neutrino mean free path 1–2.5 times while the latter decreases it 2–3 times depending on the DHF model chosen.

The DHF results are rather clustered, so that some kind of consensus should be accepted in spite of their different nature. This is a model independent conclusion as long as we work in this approximation while the DH mean free path is overestimated in comparison with those obtained in DHF models. The mixing model is the one which leads to the most different and smallest neutrino mean free paths versus the other models. The great contribution of the pseudoscalar part of the pion is responsible for this mechanism.

The underlying mechanism that accounts for these results is connected with the density of states around the Fermi surface, which is different in both approximations. Likewise the DHF nucleon self-energies differ drastically among the models. However, they lead to close results, which may be well understood by inspecting their respective relativistic effective masses. It is the way the slopes of the self-energies combine among each other, and not their absolute magnitudes, that really matters as it is evident in the vectorlike self-energies. The nucleon scalar effective mass is not able to explain these results since it only takes into account the nucleon scalar self-energy. To study systems as the NS it is more significant to use the relativistic effective mass as a nuclear observable rather than the scalar effective mass.

Therefore, one can conclude that neutrino propagation is quite sensitive to the behavior of the relativistic nucleon effective mass. The tendency in all the DHF models is to reach the population inversion at a certain model dependent density. Whether or not this phenomenon takes place depends on the stability of the star. Whenever it occurs, the NS matter would become completely opaque to the neutrino propagation.

On the contrary, compression modulus has scarce influence on the neutrino propagation. It seems rather difficult to obtain information about this nuclear observable in dense matter from the neutrino signal. Symmetry energy is not negligible due to its impact on the NS composition.

It is desirable to extend this development, by using the same DHF models, at finite temperature to study whether the strong dependence on the density of states is conserved too. This extension would allow to deal with earlier stages of the neutrino propagation involving higher neutrino energies and momentum transfers. It is also interesting, on the basis of these models, to include RPA and elucidate the differences observed from DHF with and without RPA outcome.

Another topic to deal with is the influence of a ferromagnetic phase, as the one predicted in these models, upon the neutrino propagation. To investigate whether the underlying mechanisms responsible of the appearance of this phase are also relevant in the neutrino diffusion.

If the quality of a model proceeds from its predictions about the nuclear matter observables and finite nuclei properties, then the Brueckner-DHF self-energies might be used as the best ones to trust in. In this sense, the derivative model treated here would be quite reasonable as its self-energies are in good agreement with the corresponding to the Brueckner-DHF model [19] as functions of the nuclear density, up to $2\rho_0$ (for symmetric nuclear matter). However, the lack of experimental data does not guarantee that new phenomena might appear at high densities, which are not envisaged by the simple extrapolation of the results from ordinary densities to extreme ones.

ACKNOWLEDGMENTS

This work was supported in part by Contract No. DGESIC PRB97-0360 (Spain).

APPENDIX

Using vector current conservation and translational invariance, the vector piece of the density dependent part of $\Pi_{\mu\nu}$ in Eq. (7) has only two independent components, namely, the longitudinal and transverse polarizations [26]. Their contributions to $F_{\mu\nu}$ of Eq. (10) are

$$F^L_{\mu\nu}=\frac{q^2_\mu}{2q^2}[E^*_p E^*_{p'}+M^*_p M^*_{p'}+\vec{p}^*\cdot(\vec{p}+\vec{q})^*] \quad \text{(A1)}$$

and

$$F^T_{\mu\nu}=\frac{1}{2}(M^*_p M^*_{p'}-E^*_p E^*_{p'}+p^{*2}x^2+\vec{p}^*\cdot\vec{q}). \quad \text{(A2)}$$

The axial piece can be written as the sum of the vector piece and a correction term which can be written as

$$F^A_{\mu\nu}=M^*_p M^*_{p'} g_{\mu\nu} \quad \text{(A3)}$$

and the vector-axial piece is found to be

$$F^{VA}_{\mu\nu}=\frac{q^2_\mu}{4q^2 M^*_p}(E^*_p M^*_{p'}+E^*_{p'} M^*_p)\, i\epsilon_{\mu\nu\alpha 0} q^\alpha, \quad \text{(A4)}$$

q^2_μ being the square of the four-momentum transfer.

[1] K. Hirata *et al.*, Phys. Rev. Lett. **58**, 1490 (1987).
[2] W. Keil and H. T. Janka, Astron. Astrophys. **296**, 145 (1995).
[3] C. J. Horowitz and K. Wehrberger, Nucl. Phys. **A531**, 665 (1991).
[4] S. Reddy and M. Prakash, Astrophys. J. **478**, 689 (1997).
[5] S. Reddy, M. Prakash, and J. M. Lattimer, Phys. Rev. D **58**, 13 009 (1998).
[6] S. Reddy, M. Prakash, J. M. Lattimer, and J. A. Pons, Phys. Rev. C **59**, 2888 (1999).
[7] D. Tubbs and D. Schramm, Astrophys. J. **201**, 467 (1975).
[8] R. F. Sawyer, Phys. Rev. D **11**, 2740 (1975).
[9] N. Iwamoto and C. J. Pethick, Phys. Rev. D **25**, 313 (1982).

[10] C. J. Horowitz and K. Wehrberger, Phys. Rev. Lett. **66**, 272 (1991).
[11] C. J. Horowitz and K. Wehrberger, Phys. Lett. B **226**, 236 (1992).
[12] G. Fabri and F. Matera, Phys. Rev. C **54**, 2031 (1996).
[13] N. K. Glendenning, *Compact Stars. Nuclear Physics, Particle Physics and General Relativity* (Springer, Berlin, 1997).
[14] J. M. Lattimer, C. J. Pethik, M. Prakash, and P. Haensel, Phys. Rev. Lett. **66**, 2701 (1991).
[15] A. Bouyssy, J.-F. Mathiot, Nguyen Van Giai, and S. Marcos, Phys. Rev. C **36**, 380 (1987).
[16] P. Bernardos, S. Marcos, R. Niembro, and M. L. Quelle, Phys. Lett. B **356**, 175 (1995).
[17] P. Bernardos, R. J. Lombard, M. López-Quelle, S. Marcos, and R. Niembro, Phys. Rev. C **62**, 024314 (2000).
[18] F. Gross, K. M. Maung, J. A. Tjon, L. W. Townsend, and S. J. Wallace, Phys. Rev. C **40**, R10 (1989).
[19] B. ter Haar and R. Malfliet, Phys. Rep. **149**, 207 (1987).
[20] J. R. Oppenheimer and G. M. Volkoff, Phys. Rev. **55**, 374 (1939).
[21] S. Weinberg, Phys. Rev. Lett. **19**, 1264 (1967).
[22] A. Salam, in *Elementary Particle Theory: Relativistic Groups and Analiticity*, Nobel Symposium No. 8, edited by N. Svartholm (Almqvist and Wiksell, Stockholm, 1968).
[23] A. L. Fetter and J. D. Walecka. *Quantum Theory of Many-Particle Systems* (McGraw Hill, New York, 1971).
[24] M. López-Quelle, S. Marcos, R. Niembro, A. Bouyssy, and Nguyen Van Giai, Nucl. Phys. **A483**, 479 (1988).
[25] B. D. Serot and J. D. Walecka, Adv. Nucl. Phys. **16**, 137 (1986).
[26] S. A. Chin, Ann. Phys. (N.Y.) **108**, 301 (1977).